

Seismic modeling and analysis of the prototype heated nuclear waste storage tunnel, Yucca Mountain, Nevada

Steven Smith* and Roel Snieder, Colorado School of Mines, Center for Wave Phenomena

SUMMARY

The 1997-2002 Yucca Mt. heated drift scale test (DST) used a system of heaters to simulate thermal effects from stored nuclear waste on a tunnel and groundwater flow in volcanic tuff. Seismic calibration shots were recorded on a receiver array installed around the tunnel while the tunnel wall was heated to approximately 200°C. Receiver gathers show classic wave propagation behavior for cylinders/tunnels. However, thermal/groundwater processes cause changes in the direct P-S arrival separation as temperature increases. The seismic waveforms do not change once the final wall temperature is reached. Granite wavespeed measurements were used as a physical analog to develop $V_{p,s}(x, z, t, T)$ models for Yucca Mt. tuff. Barring 3-D reflections, 2-D spectral element wave modeling coupled with constrained thermal models has replicated receiver data in the calibration source plane. Waveforms using velocity model sets with a $V^{-1}dV/dT$ gradient of -0.5% per 100°C show improved agreement with field data over those with a -2.5% per 100°C gradient. This optimal velocity change is lower than values stated in literature. Because the velocity gradient is small, velocity changes may be controlled by fracturing due to thermal expansion and fragment compression, not large bulk modulus changes associated with groundwater phase transitions. Numerical modeling also shows a diffracted wave propagating perpendicular to the tunnel wall. This wave is present in field and model data with propagation speeds varying with temperature. Therefore, P-S separation and the diffracted wave can potentially be used to monitor conditions near the tunnel.

INTRODUCTION

This work discusses the processing, analysis and modeling of seismic data collected during the second through fourth years of the 1998-2002 heated drift scale test (DST) at the Yucca Mountain facility, 90 miles NW of Las Vegas, NV (Tsang *et al.*, 1999; Rutqvist, 2004; TRW Environmental Safety Systems, Inc., 1998). Over four years the tunnel was heated to approximately 200°C by two sets of heating elements to simulate thermal emission from decaying nuclear waste. One set of heaters is a group of canisters located along the axis of the tunnel, with the second set of “wing” heaters extending 15 meters into the rock on either side (Figure 1(a)). Seismic check/calibration shots were collected to verify the functionality of a receiver array installed to monitor seismic activity (Figure 1(b))(Lehtonen, 2005; Rutledge *et al.*, 2003). Seismic data show an increasing separation between P and S wave arrivals with increasing temperature. We hypothesize that P-S separation is a function of temperature in the surrounding rock and use parametric velocity models based on ground-truth data

to model and compare waveforms with the field data. This modeling constrains in-situ velocity changes in the rock to approximately -0.5% of ambient velocity per 100°C.

FIELD DATA PROCESSING AND TRENDS

A joint effort by the U.S. national labs collected seismic data about the 47.5 meter long, 5 meter diameter tunnel using receivers locations shown by the triangles in Figure 1(b). Each receiver is a single-component instrument assumed to be aligned along the axis of the radially oriented borehole. The seismic source was a sledgehammer located in the adjoining instrumentation/observation drift 28 meters away, and six meters above the axis of the experimental drift (Figure 1(a)) (TRW Environmental Safety Systems, Inc., 1998; Rutledge, 2006). Calibration shots comprising the data set were used to check the functionality of the array after it failed to record during the first year of heating. We processed the data to remove of coherent, bandlimited noise and spurious samples (deglitching). Waveforms recorded on the same day were then stacked. Because the raw data lack a trigger signal, waveforms were aligned by first breaks for correlation analysis. This analysis revealed the P-S separation trends evident in Figure 2. Increasing P-S separation occurs up to approximately two years into the experiment. Around that date temperature stabilizes to within 20°C of the 200°C target temperature and the P-S separation remains roughly constant. This trend is observed to varying extent in all of the processed receiver gathers, and we hypothesize that the trend is caused by changing wavespeeds in the neighborhood of the tunnel resulting from thermal effects and changing groundwater saturation.

VELOCITY MODELING

2D Elastic waveform modeling was conducted to constrain wavespeed changes in the surrounding rock. Ground-truth data consisting of temperature versus radius curves at 12 month intervals above and below the tunnel (Rutqvist, 2004) permits the definition of the temperature at the tunnel wall (Figure 3(a)) and minor/vertical axis of an elliptical thermal zone caused by the core and “wing” heaters (Figure 1(a)). Ellipticity of velocity models is based on a published thermodynamic model of the transition zone at 12 months (Rutqvist, 2004), and is assumed to remain constant at temperatures/events. Wavespeed as a function of temperature from two separate sets of measurements on granite were used as physical analog for the Yucca Mountain tuff (Figures 3(b) and 3(c)). Only the section of the hysteresis cycle of Figure 3(c) indicated by the arrow was used in the second model. Granite is used to model tuff because both are igneous rocks with 65 – 75% quartz content

Yucca Mt. tunnel seismic

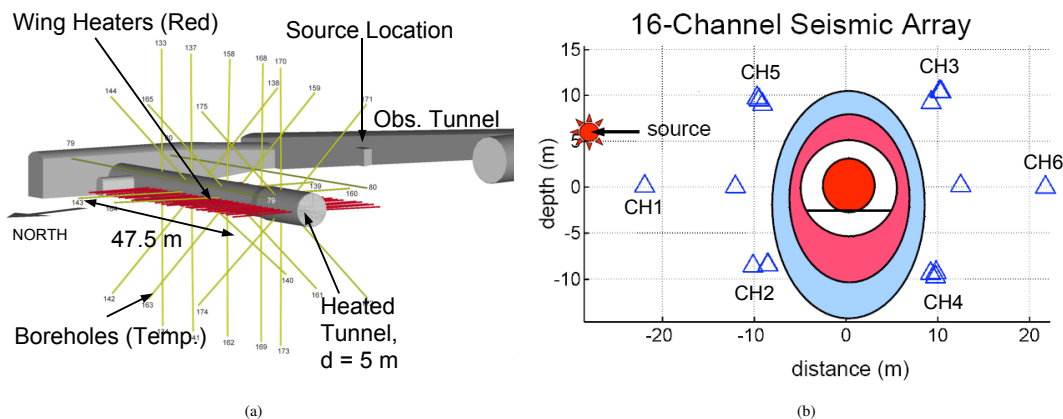


Figure 1: (a) 3-D Visualization of Yucca Mountain DST tunnel from Rutqvist (2004) showing experimental tunnel with temperature monitoring boreholes and “wing” heaters. Seismic source (sledgehammer) location is in nearby observation tunnel. (b) Seismic array receiver locations (triangles), distributed along the length of DST tunnel (end-on view). Labeled receivers used on this study are in the plane of the source (CH1 to CH6). Shaded regions around waste package (center/red) indicate hypothetical groundwater dryout (near, red), and phase transition (medium,blue) after Spycher(2003).

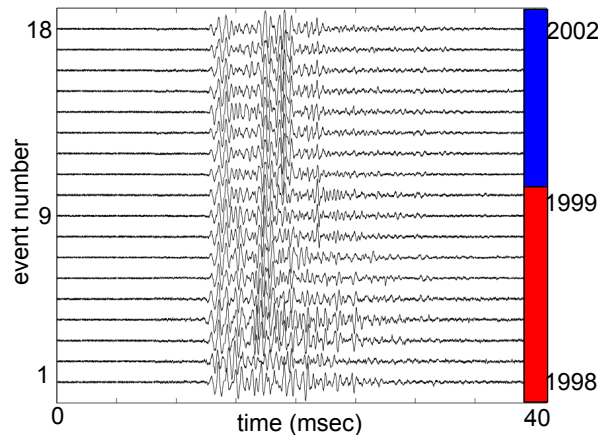


Figure 2: Receiver gather for instrument opposite tunnel from source, chronologically from bottom to top (years on right). Note increasing separation of primary (compressional) and secondary (shear) arrivals during heating of the tunnel (indicated by red bar) that remain fixed through period of maximum operating temperature of 200°C (blue bar), indicating changes to the rock occurring during tunnel heating.

(Carmichael, 1989; Grêt *et al.*, 2006). Grain size is not considered a primary velocity control as fracturing occurs both around and through grains at sufficiently high temperatures and pressures (Batzle *et al.*, 1980). Because the data lacks a trigger, measurements of differential path-lengths vs. arrival times were used to determine an ambient compressional velocity of approximately 3600 m/s. This value agrees well with ambient velocities of Yucca Mountain Topopha tuff given by New England Research (New England Research, 2007) and Indian Springs tuff from the Mines Commonground Database (Batzle & Scales, 2001-present). Polynomial coefficients of the granite data fit were adjusted to match the ambient velocity of tuff from the differential travel times, generating velocity vs. temperature models for tuff. These models have V_p slopes of -0.5% and -2.5% with respect to ambient velocities over a 100°C temperature domain. V_s is determined from the $-0.5\%/100^\circ\text{C}$ data. Red squares in Figure 3(a) indicate days/temperatures where calibration shot data is available. Note that the seismic calibration shots do not begin at ambient temperature/velocity conditions or continue into the cooling phase when the heaters were shut down.

MODEL/DATA COMPARISON

Model waveforms were generated using SEM2DPACK spectral element software (Ampuero, 2007), a 2D package that limits analysis to the receivers in the plane of the source. Spectral element modeling (Komatitsch & Tromp, 1999) uses a variational integral formulation and interpolating polynomials across computational mesh elements to solve for displacement. It does not suffer from much of the dispersion effects and numerical instabilities seen in finite element and finite difference algorithms associated with grid/mesh spacing or interpolation errors (Juhlin, 1995; Levander, 1988; Virieux, 1986; Muir *et al.*, 1992). Potential, but less useful methods include smoothing

Yucca Mt. tunnel seismic

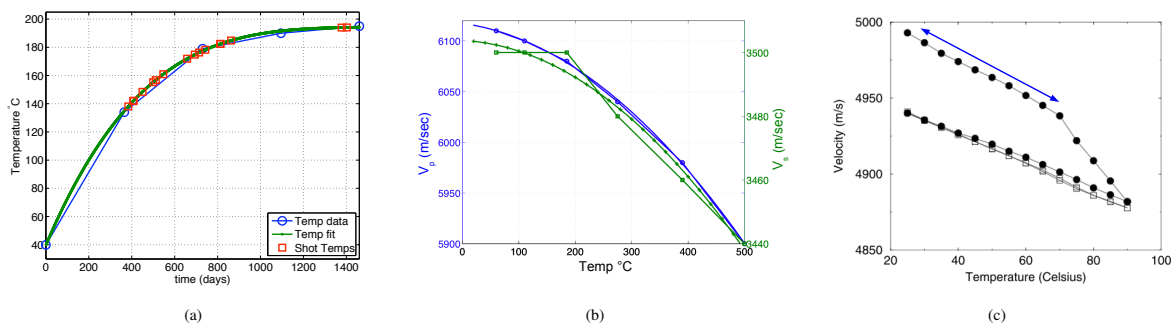


Figure 3: Velocity modeling data as described in the text. (a) Tunnel wall temperature. Red squares indicate days where calibrations shots were recorded. (b) Granite $V_{p,s}$ data and fit from Carmichael (1989) yielding $-0.5\%/100^\circ\text{C}$ model for tuff. (c) Granite V_p data from Grêt *et al.* (2006) yielding $-2.5\%/100^\circ\text{C}$ model for tuff.

of interfaces and Rotated Staggered Grids, which still require a high number of points per wavelength (Saenger *et al.*, 2000; Bohlen & Saenger, 2006). Minor variations between model and field waveforms exist due to reflection and scattering by the connecting access tunnel.

Good agreement between modeled data (heavy/blue) and field data (thin/black) is shown in Figure 4(a). The data shown include all calibration events for a receiver with a source/receiver path crossing most of the thermal transition zone (CH4). Figures 4(b) and 4(c) show alignment of shear wave arrivals for the -0.5% and -2.5% per 100°C tuff models respectively. Field data waveforms are the output of the preprocessing stage and have been aligned to the first break of the model data for each event. The vertical line across the shear wave arrivals serves as a reference for the central peak of both model and field waveforms (heavy and thin lines respectively). Acceptable agreement between modeled and field waveforms was achieved for models with -1% change for the total temperature range of 200°C , as shown in Figure 4(b) ($-0.5\%/100^\circ\text{C}$). This alignment can be contrasted with the $-2.5\%/100^\circ\text{C}$ velocity change shown in Figure 4(c) where the arrival time of the shear wave clearly increases. The $-0.5\%/100^\circ\text{C}$ temperature change is less than numbers stated in literature (Guéguen & Palciauskas, 1994), and clearly constrain the *in-situ* changes of velocity to be small. This suggests that the controlling factor of wavespeed change is fracturing caused by thermal expansion or compression of fragments trapped in existing fractures (Batzle *et al.*, 1980). Occurrence of fracturing is supported by the localization of microseisms by Rutledge *et al.* (Rutledge *et al.*, 2003). Were water present in the fractures surrounding the tunnel, the total bulk modulus could vary by several orders of magnitude, resulting in a much higher wavespeed in the transition zone (Wang, 2001). Unfortunately, as seismic data was not collected from ambient temperature and velocity conditions, we can't study potential effects of groundwater entering/re-entering the surroundings. Also, without cooling cycle data, we cannot determine if microfracture damage occurs as demonstrated by the change in slope of the top branch of the hysteresis data used for velocity modeling (Figure 3(c)) (Grêt *et al.*, 2006).

In addition to constraints on the velocity, numerical modeling shows the presence of a diffracted wave ("Franz" wave) propagating perpendicular to the surface of the tunnel in the shadow zone. This wavefront has been described analytically (Glibert & Knopoff, 1959) and observed experimentally (Neubauer & Dragonette, 1970), and is clearly seen in modeled data (Figure 5(a)). Subtle indications of the Franz wave in the Yucca Mt. seismic can be observed by comparing arrivals in modeled shot gathers with wavelet variations in receiver gathers. However, poor signal-to-noise ratios (SNR) at later times in the field data preclude it from analysis. Low Franz wave SNR occurs because the receiver array did not include elements located sufficiently close to the thermal transition zone. Franz wave sensitivity to velocity changes near the tunnel suggests that future monitoring of rock conditions may be achieved by observing transit times around the surface of the tunnel or differential arrival times of the curved wavefront by a linear array extending radially from the tunnel wall (Figure 5(b)).

DISCUSSION/CONCLUSIONS

Processing of seismic data from the heated drift scale test (DST) of 1998-2002 shows clear changes in P-S wavelet separation vs time and temperature. Multiple velocity models based on granite and adjusted to meet ambient velocity values were used to model waveforms at receivers in a plane with seismic source. Good agreement with wavespeed models having $-0.5\%/100^\circ\text{C}$ velocity change from ambient values constrains velocity changes due to heating to be quite weak. The velocity change is likely due to additional fracturing caused by compression of fragments trapped in existing fractures during thermal expansion. Sufficient amounts of groundwater would cause a large bulk modulus/velocity changes. Localizations of induced seismicity support thermal expansion/fracturing as the primary velocity control (Rutledge *et al.*, 2003). Diffracted phases propagating in the shadow zone of the tunnel may be useful monitoring tools if the proper receiver array is installed. **Acknowledgement:** This work was supported by the Office of Basic Energy Science of the Department of Energy through grant DE-FG02-06ER15778.

Yucca Mt. tunnel seismic

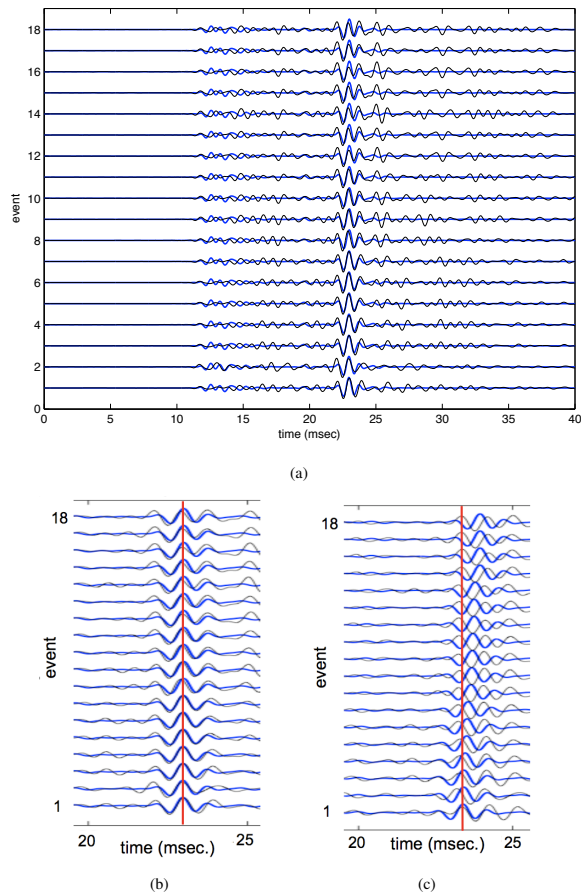


Figure 4: (a) Comparison of CH4 model (heavy/blue) vs. field data (thin/black) for temperature change of $-0.5\%/100^\circ\text{C}$ with respect to ambient temperature and velocity. Calibration/check-shot event numbers on vertical axis increase with time/tunnel wall temperature, beginning on Dec. 3, 1998, and concluding Jan. 14, 2002. See Figure 1(b) for receiver location. (b) and (c) Shear wave arrival shot gathers for extrapolated tuff data having $-0.5\%/100^\circ\text{C}$ (b) and $-2.5\%/100^\circ\text{C}$ (c) slopes, respectively. Model waveforms are darker, heavier traces. Data is from Channel 4, located below tunnel opposite from source. Both figures show increasing time/temperature as a function of event number, chronologically from top to bottom. Shear wave arrivals show good agreement for models based on -0.5% per 100°C slope. Note: all field and model waveforms in (b), right, arrive at later times because all field waveforms are aligned with model waveforms computed using a higher dV/dT than (a) left ($-2.5\%/100^\circ\text{C}$ vs. $-0.5\%/100^\circ\text{C}$).

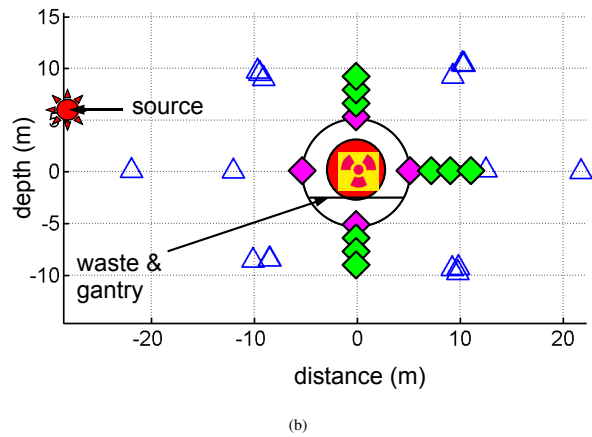
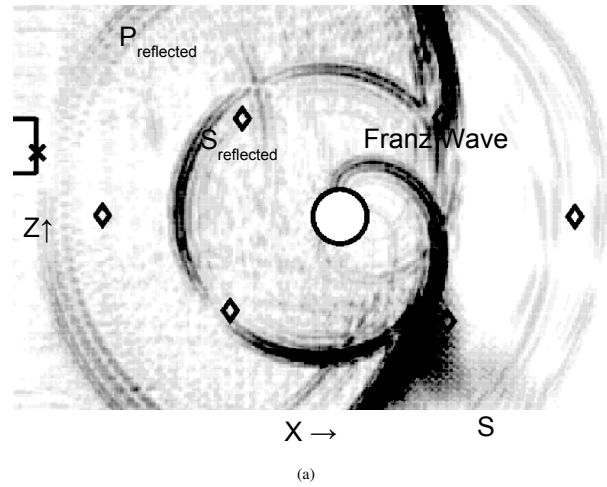


Figure 5: (a) Numerical modeling shows diffracted/Franz wave propagating over tunnel crown normal to the tunnel surface. (b) Because this wave circles the tunnel in within the zone most effected by thermal change, its arrival time around the tunnel and differential arrival times vs. radius are potential tools for monitoring using the suggested array configurations (diamonds).

Yucca Mt. tunnel seismic

REFERENCES

- Ampuero, Jean-Paul. 2007 (February). *SEM2DPACK: A Spectral Element Method for 2D wave propagation and fracture dynamics, with emphasis on computational seismology and earthquake source dynamics*. v 2.2.7 edn. ETH Zürich (Swiss Federal Institute of Technology), Institute of Geophysics, Seismology and Geodynamics Group, ETH Hönggerberg HPP O 13.1, CH-8093 Zürich, Switzerland. <http://sourceforge.net/projects/sem2d/>.
- Batzle, M. L., Simmons, G., & Sigfried, R. W. 1980. Microcrack Closure in Rocks Under Stress: Direct Observation. *J. Geophysical Research*, **85**(B12), 7072–7090.
- Batzle, Mike, & Scales, John. 2001-present. *Mines Commonground Database*. Colorado School of Mines, <http://commonground.mines.edu/>. A free archive and database of rock properties measurements.
- Bohlen, Thomas, & Saenger, Erik. 2006. Accuracy of Heterogeneous Staggered-Grid Finite-Difference Modeling of Rayleigh Waves. *Geophysics*, **71**(4), T109–T115.
- Carmichael, R. S. (ed). 1989. *CRC Practical Handbook of Physical Properties of Rocks and Minerals*. CRC Press.
- Glibert, F., & Knopoff, L. 1959. Scattering of Impulsive Elastic Waves by a Rigid Cylinder. *J. of the Acoustical Society of America*, **31**(9), 1169–1175.
- Grêt, A., Snieder, R., & Scales, J. 2006. Time-lapse Monitoring of Rock Properties with Coda Wave Interferometry. *J. Geophysical Research*, **111**(B03305), doi:10.1029/2004JB003354.
- Guéguen, Yves, & Palciauskas, Victor. 1994. *Introduction to the Physics of Rocks*. Princeton University Press.
- Juhlin, Chris. 1995. Finite-Difference Elastic Wave Propagation in 2-D Heterogeneous Traversely Isotropic Media. *Geophysical Prospecting*, **43**(August), 843–858.
- Komatitsch, Dimitri, & Tromp, Jeroen. 1999. Introduction to the Spectral Element Method for Three-Dimensional Seismic Wave Propagation. *Geophysics Journal International*, **139**, 806–822.
- Lehtonen, Aleksis. 2005 (November). *Evaluation of Rock Stress Estimation by the Kaiser Effect*. Working Report 2005-67. Posiva Oy, FL-27160 Olkiluoto, Finland.
- Levander, Alan. 1988. Fourth-Order Finite-Difference P-SV Seismograms. *Geophysics*, **53**(11), 1425–1436.
- Liu, Y., Wu, R., & Ying, C. 2000. Scattering of Elastic Waves by an Elastic or Visoelastic Cylinder. *Geophys. J. Int.*, **142**, 439–460.
- Muir, F., Dellinger, J., Etgen, J., & Nichols, D. 1992. Short Note: Modeling Elastic Fields Across Irregular Boundaries. *Geophysics*, **7**(9), 1189–1193.
- Neubauer, Werner, & Dragonette, Louis. 1970. Observation of Waves Radiated from Circular Cylinders Caused by an Incident Pulse. *J. of the Acoustical Society of America*, **48**(5), 1135–1149.
- New England Research. 2007. *Bulk and Mechanical Properties of Paintbrush Tuff from Yucca Mountain, NV*. Tech. rept. New England Research, contact: info@ner.com, 802-296-2401, http://nersolutions.com/pdf/NER.tn_paintbrush_tuff.pdf.
- Rutledge, J. 2006 (February). *Personal Communication (LANL)*. E-mail.
- Rutledge, J., Roe, C., Peterson, J., & Majer, E. 2003 (August). *Relocation of Yucca Mountain Induced Microseismicity*. Tech. rept. Los Alamos National Laboratory, Earth and Environmental Sciences Division, EES-11 Geophysics.
- Rutqvist, J. 2004 (November). *Drift Scale THM Model*. Tech. rept. MDL-NBS-HS-000017 REV00. Office of Civilian Radioactive Waste Management.
- Saenger, Erik, Gold, Norbert, & Shapiro, Serge. 2000. Modeling the Propagation of Elastic Waves Using a Modified Finite-Difference Grid. *Wave Motion*, **31**, 77–92.
- Spycher, N.F., Sonnenthal, E.L., & Apps, J.A. 2003. Fluid Flow and Reactive Transport Around Potential Nuclear Waste Emplacement Tunnels at Yucca Mountain, Nevada. *J. of Contaminant Hydrology*, **62-63**, 653–673.
- TRW Environmental Safety Systems, Inc. 1998 (July). *Drift Scale Test As-Built Report*. Tech. rept. BAB000000-01717-5700-00003 REV 01. Civilian Radioactive Waste Management System Management and Operating Center, TRW/US DOE. Contract Number DE-AC08-91RW00134.

Yucca Mt. tunnel seismic

- Tsang, Y. W., Apps, J., Berkholzer, J. T., Peterson, J. E., Sonnenthal, E., Spycher, N., & Williams, K. H. 1999. *Yucca Mountain Drift Scale Test Progress Report*. Tech. rept. LBNL-42538. Lawrence Berkley National Laboratory, Earth Sciences Division.
- Virieux, Jean. 1986. P-SV Wave Propagation in Hetrogeneous Media: Velocity Stress Finite-Difference Method. *Geophysics*, **51**(4), 889–901.
- Wang, Z. 2001. Y2K Tutorial: Fundamentals of Seismic Rock Physics. *Geophysics*, **66**(2), 398–412.